Antenna Scanning Techniques for Estimation of Spacecraft Position

Wodek Gawronski[1] and Emily M. Craparo[2]

[1]Jet Propulsion Laboratory, California Institute of Technology, MS 238-528
4800 Oak Grove Drive, Pasadena, CA 91109 USA
Tel.: +1 (818) 354-1783; Fax: +1 (818) 393-0207; E-mail: Wodek.K.Gawronski@jpl.nasa.gov

[2]Massachusetts Institute of Technology
Cambridge, MA 02139 USA

Abstract

Scanning movements are added to a tracking antenna's trajectory to estimate the true spacecraft position. The scanning movements are composed of the harmonic axial movements of an antenna. This motion produces power variations of the received signal, which are used to estimate the spacecraft's position. Three different scanning patterns (conical scan, Lissajous scan, and rosette scan) are presented and analyzed in this paper. The analysis includes the evaluation of the estimation errors due to random or harmonic variation of the antenna's position, and due to random and harmonic variations of the power level. Typically, the estimation of the spacecraft's position is carried out after completing a full scanning cycle. Sliding-window scanning is introduced in this paper, wherein the spacecraft-position estimation is carried out in an almost-continuous manner, and it reduces the estimation time by half.

Keywords: Antennas; scanning antennas; tracking; space vehicle tracking; satellite tracking; conical scan; Rosette scan; Lissajous scan; spacecraft position; antenna mechanical factors

1. Introduction

The NASA Deep Space Network antennas serve as communication tools for space exploration. They are used to send commands to spacecraft and to receive information collected by spacecraft. The spacecraft trajectory (its position as a function of time) is typically known with high accuracy, and this trajectory is programmed into the antenna, forming the antenna command. [the term "antenna command" refers to the combination of the series of position-movement instructions given to the antenna, and the resulting sequence of motions through which the antenna is thereby commanded; it is assumed that the antenna motion ideally follows the commands]. However, due to environmental disturbances, such as temperature gradient, wind and gravity forces, and manufacturing imperfections, the antenna does not point precisely towards the spacecraft. These disturbances are difficult or impossible to predict, and therefore must be measured before compensatory measures can be taken. A technique commonly used for the determination of the true spacecraft position is the conical-scanning method (conscan). During conscan, circular movements are added to the antenna command, as shown in Figure 1. These circular movements cause sinusoidal variations in the power of the signal from the spacecraft received by the antenna, and these variations are used to estimate the true spacecraft position.

The radius of the conscan movement is typically chosen such that the loss of the signal power is of the order of 0.1 dBi. Thus, it depends on the frequency of the receiving signal. For Ka-band (32 GHz) signals, the conscan radius is 1.55 mdeg. Depending on the radius, the sampling rate, the antenna's tracking capabilities, and the desired accuracy, the period of the conscan typically varies from 30 to 120 s (in our case, it will be 60 s). Finally, the sampling frequency was chosen as 50 Hz to match the existing Deep Space Network antenna-sampling frequency, and to satisfy the Nyquist criterion, which says that the sampling rate shall be at least twice the antenna's bandwidth (of 10 Hz).

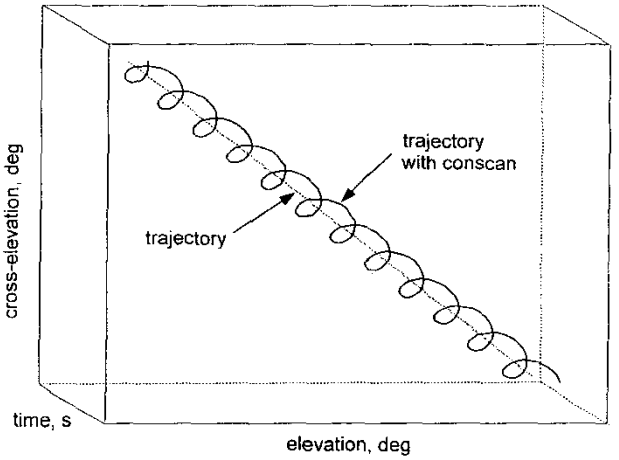

Figure 1. A schematic diagram of the spacecraft trajectory and the antenna conscan. The relative size of the conscan radius has been exaggerated.

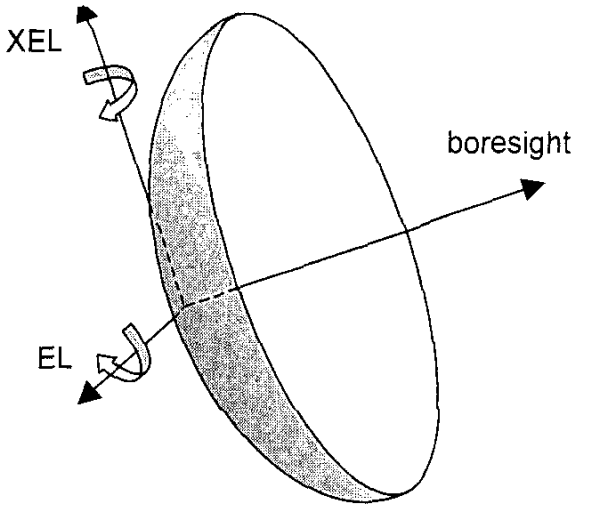

Figure 2. The elevation and cross-elevation coordinate system.

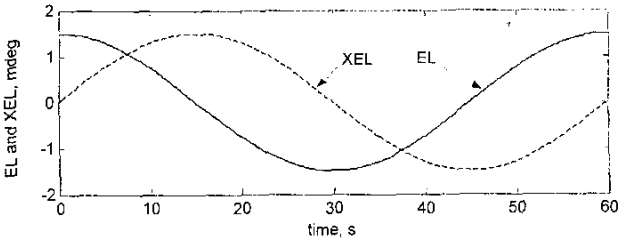

Figure 3. The elevation and cross-elevation components of the conscan.

The conscan technique is used for antenna and radar tracking (see Damonte and Stoddard [1] and Bierson [2]), and for spacecraft applications (as described by Ohlson and Reid [3], Alvarez [4], and Eldred [5]). For missile tracking, it is described in [6]. The rosette scanning is used in missile tracking (see [6]), and in telescope infrared tracking (see [7]). The paper being presented is a development of the least-square and Kalman-filter techniques [4, 5]. It also introduces and analyzes sliding-window conscan, Lissajous scanning, and rosette scanning, and describes the scans' responses to various disturbances.

2. Power Variation During Conscan

Let us begin by defining a coordinate system with its origin located at the antenna-command position (i.e., translating with the antenna command). The coordinate system consists of two components: the elevation rotation of the dish and the cross-elevation rotation of the dish. The first component is defined as a rotation with respect to a horizontal axis orthogonal to the boresight, and the second as a rotation with respect to a vertical axis orthogonal to the boresight and elevation axis (see Figure 2). Since the spacecraft position in this coordinate system is measured with respect to the antenna boresight, and the spacecraft trajectory is accurately known, its position deviations are therefore predominantly caused by either unpredictable disturbances acting on the antenna (e.g., wind pressure), or by antenna deformations (such as thermal deformations, and un-modeled atmospheric phenomena, such as refraction). During conical scanning, the antenna moves in a circle of radius r, with its center located at the antenna-command position.

The conscan data are sampled with a sampling frequency of 50 Hz. Thus, the sampling time is $\Delta t = 0.02$ s. The sampling rate was chosen to exceed the doubled antenna bandwidth of 10 Hz. The antenna position, a_i, at time $t_i = i\Delta t$ consists of the elevation component, a_{ei}, and the cross-elevation component, a_{xi}, as shown in Figure 3. The position is described by the following equation:

$$a_i = \begin{Bmatrix} a_{eli} \\ a_{xeli} \end{Bmatrix} = \begin{Bmatrix} r\cos\omega t_i \\ r\sin\omega t_i \end{Bmatrix}. \tag{1}$$

Plots of a_{ei} and a_{xi} for $r = 1.55$ mdeg, and for a period $T = 60$ s ($\omega = 0.1047$ rad/s), are shown in Figure 3.

The target position is denoted s_i, with the elevation and cross-elevation components s_{ei} and s_{xi} (see Figure 4). The antenna-position error is defined as the difference between the target position and the antenna position, i.e.,

$$e_i = s_i - a_i. \tag{2}$$

Like the antenna position, it has two components, elevation and cross-elevation position errors:

$$e_i = \begin{Bmatrix} e_{ei} \\ e_{xi} \end{Bmatrix} = \begin{Bmatrix} s_{ei} - a_{ei} \\ s_{xi} - a_{xi} \end{Bmatrix}. \tag{3}$$

The total error at $t_i = i\Delta t$ is described as the position rms error, that is,

$$\varepsilon_i = \sqrt{e_i^T e_i} = \|e_i\|_2. \tag{4}$$

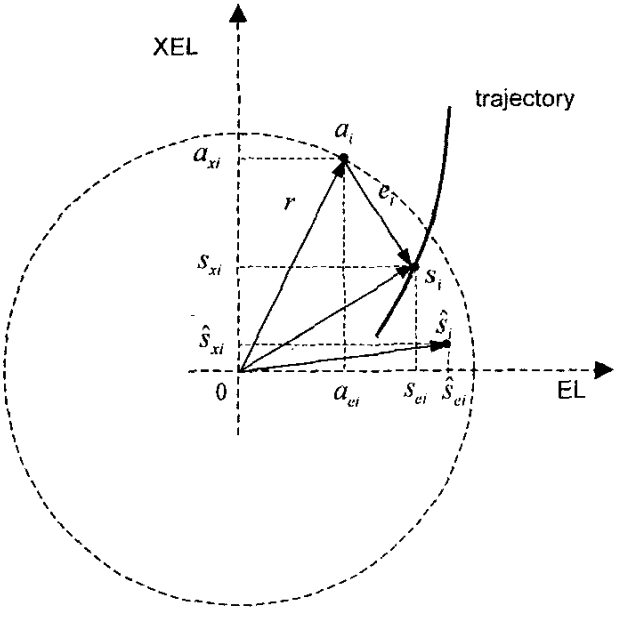

Figure 4. The antenna position, the target position, and the estimated target position during conscan.

Combining Equations (1), (2), and (4), one obtains

$$\varepsilon_i^2 = s_i^T s_i - 2a_i^T s_i + a_i^T a_i = s_i^T s_i - 2a_i^T s_i + r^2 . \qquad (5)$$

Next, we describe how the error impacts the beam power. The carrier power, p_i, is a function of the error, ε_i, and its Gaussian approximation is expressed as

$$p_i = p_{oi} \exp\left(-\frac{\mu}{h^2} \varepsilon_i^2 \right) + v_i . \qquad (6)$$

v_i is the signal noise, $\mu = 4\ln(2) = 2.7726$, and h is the half-power beamwidth of the antenna: for Ka-band, $h = 17$ mdeg. Note that although a spacecraft can move relatively quickly with respect to fixed coordinates, it typically moves slowly in the selected coordinate frame (this relative movement is caused by slowly-varying disturbances). For example, thermal deformations have periods of several hours, while the conscan period is only one minute. Therefore, it is safe to assume that the target position is constant during the conscan period, i.e., that $s_i \cong s$. We also assume that the power is constant during the conscan period, i.e., that $p_{oi} = p_o$ (where p_o is the maximum carrier power).

Using the approximation $\exp(x) \cong 1 + x$, one obtains Equation (6) as follows:

$$p_i = p_o \left(1 - \frac{\mu}{h^2} \varepsilon_i^2 \right). \qquad (7)$$

Substituting Equation (5) into the above equation, and assuming $s_i = s$, $p_{oi} \approx p_o$, one obtains

$$p_i = p_o - \frac{p_o \mu}{h^2} \left(r^2 + s^T s - 2a_i^T s \right) + v_i$$

$$= p_m + \frac{2p_o \mu}{h^2} a_i^T s + v_i ,$$

or, using Equation (1), one obtains

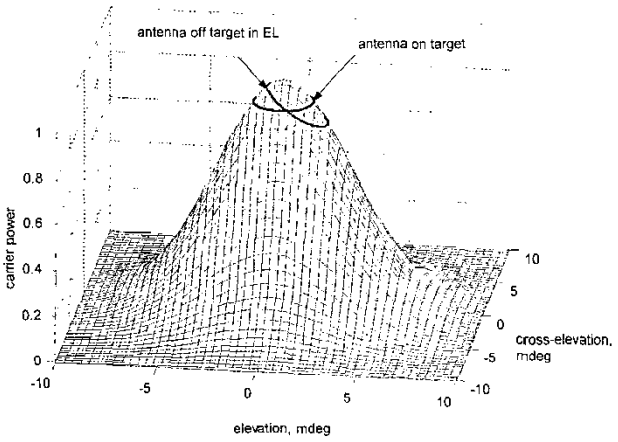

Figure 5. The carrier power and the conscan power for a perfectly pointed antenna, and for elevation error.

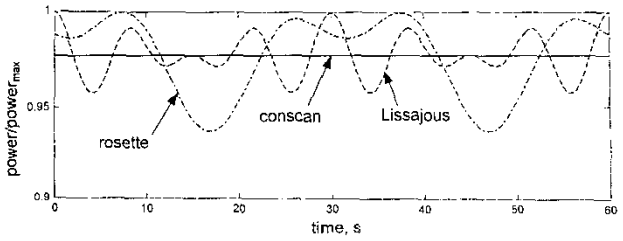

Figure 6a. A power variation (with respect to maximum power) for the conscan, Lissajous, and rosette scans when the antenna is on target.

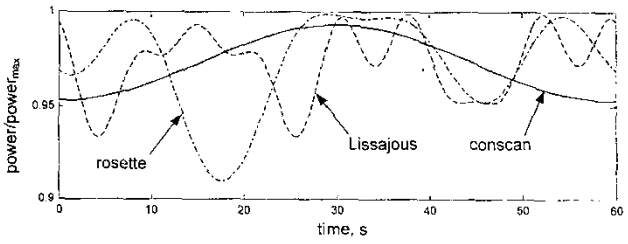

Figure 6b. A power variation (with respect to maximum power) for the conscan, Lissajous, and rosette scans when there is a 0.7 mdeg elevation error.

$$p_i = p_m + \frac{2p_o \mu r}{h^2} \left(s_e \cos \omega t_i + s_x \sin \omega t_i \right) + v_i . \qquad (8)$$

In the above equations, p_m is the mean power, defined as

$$p_m = p_o \left[1 - \frac{\mu}{h^2} \left(r^2 + s^T s \right) \right] \qquad (9)$$

(see [5]). The plot of p_i is shown in Figure 5 and Figure 6. Additionally, in these figures, the plot of the power as a function of the antenna position is marked. These plots are presented for the case of the antenna being perfectly pointed at the target, as well as for the case of an error in antenna elevation position. It can be seen that for the perfectly pointed antenna, the received power is constant, and smaller than the maximum power. For a mis-pointed antenna, the received power varies in a sinusoidal fashion, as is derived in the following paragraph.

The algorithm presented above is a corrected Alvarez algorithm [4]. Here, the Taylor expansion was taken with respect to the error ε_i, which produces the maximum power rather than mean power in the second component in Equation (8).

Denoting the variation from the mean power as $dp_i = p_i - p_m$, one obtains from Equation (8)

$$dp_i = g s_e \cos \omega t_i + g s_x \sin \omega t_i + v_i , \qquad (10)$$

where

$$g = \frac{2p_o \mu r}{h^2} . \qquad (11)$$

In this equation, g and ω are known parameters; the power varia-

tion, dp_i, is measured; and the spacecraft coordinates, s_e and s_x, are to be determined. If no noise were present, the spacecraft position could be obtained from the amplitude and phase of the power variation. Since the received power signal is noisy, the least-square technique is applied.

3. Estimating Spacecraft Position from the Power Measurements

Denoting

$$k_i = g\left[\cos\omega t_i \quad \sin\omega t_i\right], \tag{12}$$

Equation (10) can be written as

$$dp_i = k_i s + v_i, \tag{13}$$

where $s = \begin{Bmatrix} s_e \\ s_x \end{Bmatrix}$. For an entire conscan circle/period,

$$dP = \begin{Bmatrix} dp_1 \\ dp_2 \\ \vdots \\ dp_n \end{Bmatrix}, \quad K = \begin{bmatrix} k_1 \\ k_2 \\ \vdots \\ k_n \end{bmatrix}, \quad V = \begin{Bmatrix} v_1 \\ v_2 \\ \vdots \\ v_n \end{Bmatrix}, \tag{14}$$

and Equation (13) is obtained in the following form:

$$dP = Ks + V. \tag{15}$$

The estimated spacecraft position, $\hat{s}$, is the least-square solution of the above equation:

$$\hat{s} = K^{+} dP, \tag{16}$$

where $K^{+} = \left(K^T K\right)^{-1} K^T$. Consistent with the other notation, $\hat{s}_i = \begin{Bmatrix} \hat{s}_{ei} \\ \hat{s}_{xi} \end{Bmatrix}$, where $\hat{s}_{ei}$ is the elevation component of the estimated target position at $i\Delta t$, and $\hat{s}_{xi}$ is the cross-elevation component of the estimated target position at $i\Delta t$.

4. Lissajous Scans

In the Lissajous scanning pattern, the antenna position, a_i, at time $t_i = i\Delta t$ consists of the elevation component, a_{ei}, and the cross-elevation component, a_{xi}, described by the following equation:

$$a_i = \begin{Bmatrix} a_{ei} \\ a_{xi} \end{Bmatrix} = \begin{Bmatrix} r\sin n\omega t_i \\ r\sin m\omega t_i \end{Bmatrix}, \tag{17}$$

where n and m are natural numbers. Again, the components are harmonic functions, which are most desirable for the antenna motion because they do not result in jerks or rapid motions. The Lissajous curve for $r = 1.55$ mdeg, $n = 3$, and $m = 4$ is shown in Figure 7, and the individual components' plots (a_{ei} and a_{xi}) are shown in Figure 8. The radius was chosen such that the mean power loss was equal to the mean power loss resulting from a conscan sweep with $r = 1.55$ mdeg.

For this scanning pattern, the power variation is obtained as follows. With the antenna position error defined as in Equation (2), the total error at $t_i = i\Delta t$ is described as the position rms error:

$$\varepsilon_i^2 = s_i^T s_i - 2a_i^T s_i + a_i^T a_i. \tag{18}$$

Using the carrier power, p_i, as in Equation (7), and assuming that the spacecraft's position and the carrier power are constant during conscan period, i.e., that $s_i = s$ and $p_{oi} = p_o$, one obtains

$$\begin{aligned} p_i &= p_o - \frac{p_o \mu}{h^2}\left(a_i^T a_i + s^T s - 2a_i^T s\right) + v_i \\ &= p_m \exp\left(\frac{2\mu}{h^2} a_i^T s\right) + v_i \\ &= p_m \exp\left[\frac{2\mu r}{h^2}\left(s_e \sin n\omega t_i + s_x \sin m\omega t_i\right)\right] + v_i. \end{aligned} \tag{19}$$

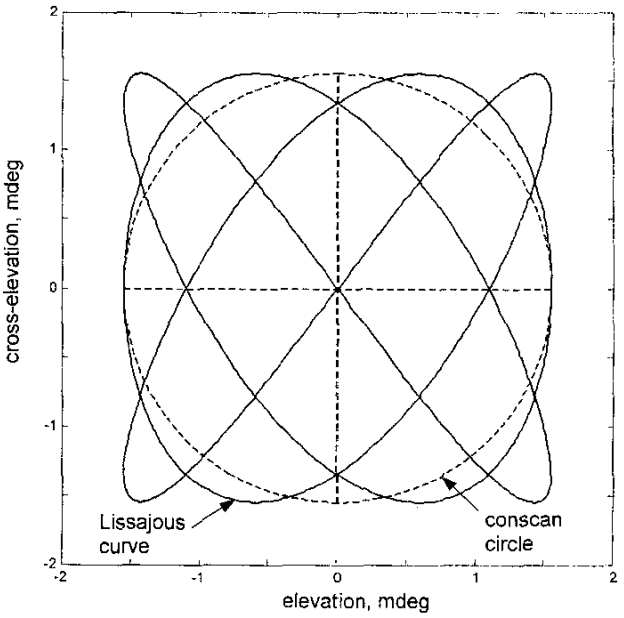

Figure 7. The Lissajous curve for $r = 1.55$ mdeg, $n = 3$, and $m = 4$.

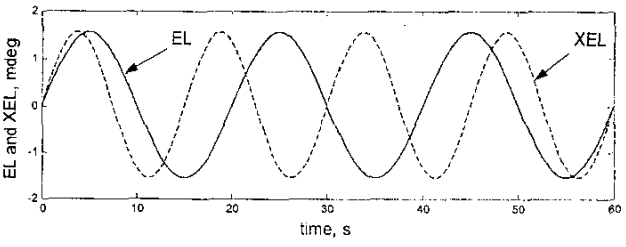

Figure 8. The elevation and cross-elevation components of the Lissajous scanning pattern for $n = 3$, $m = 4$.

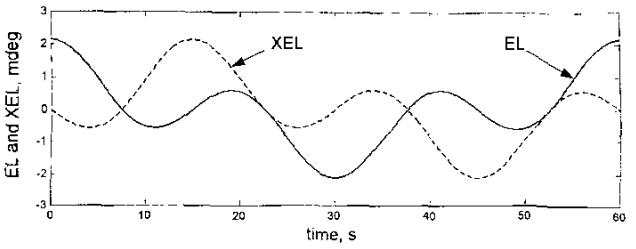

Figure 9. The rosette elevation and cross-elevation components.

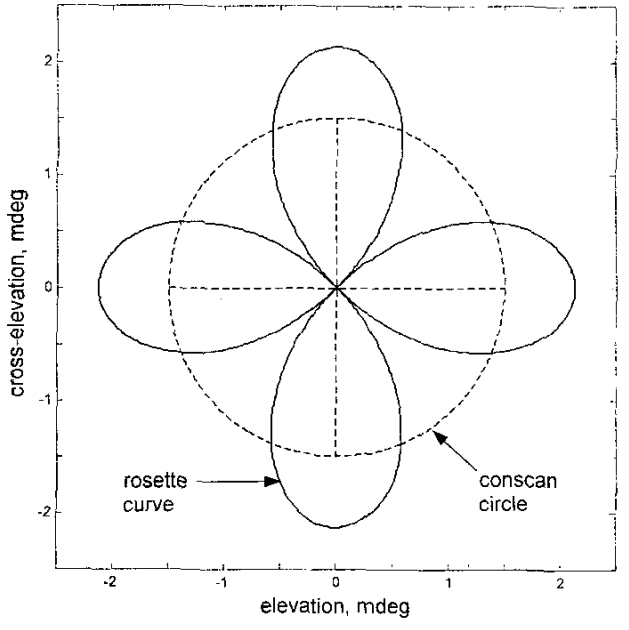

Figure 10. The rosette curve for $r = 1.1$ mdeg, $n = 1$, and $m = 3$.

Using Equation (17), one obtains

$$p_i = p_m + \frac{2p_o\mu r}{h^2}\left(s_e \sin n\omega t_i + s_x \sin m\omega t_i\right) + v_i, \qquad (20)$$

where p_m is the mean power, defined as

$$p_m = p_o\left[1 - \frac{\mu}{h^2}\left(a_i^T a_i + s^T s\right)\right]. \qquad (21)$$

Denoting the variation from the mean power as $dp_i = p_i - p_m$, one obtains the power variation as a function of the spacecraft position, s_e and s_x:

$$dp_i = gs_e \sin n\omega t_i + gs_x \sin m\omega t_i + v_i. \qquad (22)$$

In this equation, g and ω are known parameters, dp_i is measured, and s_e and s_x are the spacecraft coordinates to be determined. The plot of the power variation, dp_i, is shown in Figure 6. It is seen from this figure that power variation occurs even when the antenna is perfectly pointed, unlike the conscan situation. The Lissajous radius, however, was chosen such that on average the loss of the received power is the same as during conscan. Also, unlike the conscan situation, the maximum power is reached during the cycle, since the Lissajous curve crosses through the origin.

As in the conscan case, the spacecraft-position estimate is obtained from Equation (16). In the Lissajous case, the matrix K is changed such that its ith row is

$$k_i = g\left[\sin n\omega t_i \quad \sin m\omega t_i\right]. \qquad (23)$$

5. Rosette Scans

In the rosette scanning, the antenna movement is described by the following equation:

$$a_i = \begin{Bmatrix} a_{ei} \\ a_{xi} \end{Bmatrix} = \begin{Bmatrix} r\cos n\omega t_i + r\cos m\omega t_i \\ r\sin n\omega t_i - r\sin m\omega t_i \end{Bmatrix}. \qquad (24)$$

The plots of the elevation component, a_{ei}, and the cross-elevation component, a_{xi}, are shown in Figure 9 for the rosette curve of radius $r = 1.10$ mdeg, $n = 1$, and $m = 3$. The rosette curve itself is shown in Figure 10 (the radius was chosen such that the mean power loss is the same as for the conscan with $r = 1.55$ mdeg). Note that the rosette curve, unlike the conscan circle, crosses the origin, and thus receives peak power if the target and boresight position coincide.

Following the derivation as above, the antenna power is obtained as follows:

$$p_i = p_m + \frac{2p_o\mu r}{h^2}\left[s_e\left(\cos n\omega t_i + \cos m\omega t_i\right) + s_x\left(\sin n\omega t_i - \sin m\omega t_i\right)\right] + v_i; \qquad (25)$$

therefore, the power variation is

$$dp_i = gs_e\left(\cos n\omega t_i + \cos m\omega t_i\right) + gs_x\left(\sin n\omega t_i - \sin m\omega t_i\right) + v_i, \qquad (26)$$

where g is given by Equation (11). The plots of variations of dp_i are shown in Figure 6. The plots show that received power varies for the perfectly pointed antenna. Also, like the Lissajous case, the maximum power is reached during the cycle, since the rosette curve crosses through the origin.

The spacecraft-position estimate is determined from the above equation, using Equation (16), where the ith row of the matrix K in this equation is

$$k_i = g\left[\cos n\omega t_i + \cos m\omega t_i \quad \sin n\omega t_i - \sin m\omega t_i\right]. \qquad (27)$$

6. Performance Evaluation

The scanning performance is evaluated in the presence of disturbances. First, the antenna position is disturbed by random factors, such as wind gusts, and by deterministic disturbances, which can be decomposed into harmonic components. Secondly, the carrier power is also modeled as disturbed by random noise (receiver noise, for example), and deterministic variations, such as

Table 1. The estimation error (mdeg) due to 1 mdeg noise in EL, for spacecraft position at (0, 0).

Direction	Conscan	Lissajous	Rosette
Elevation	0.025	0.025	0.037
Cross-elevation	0.013	0.017	0.010

Table 2. The estimation error (mdeg) due to 1 mdeg noise in XEL, for spacecraft position at (0, 0).

Direction	Conscan	Lissajous	Rosette
Elevation	0.015	0.019	0.010
Cross-elevation	0.027	0.029	0.037

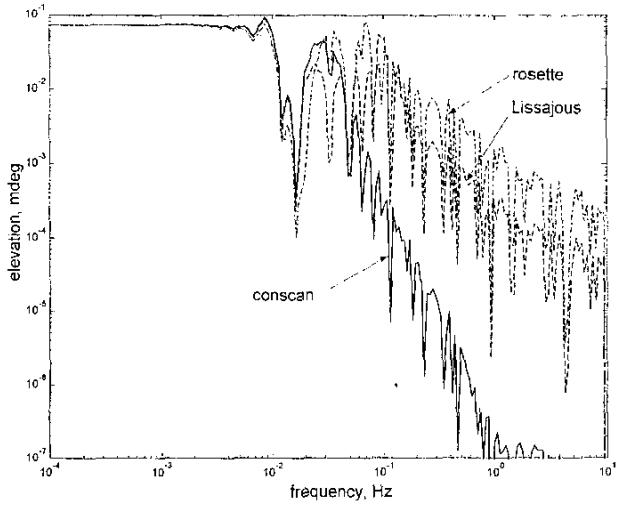

Figure 11a. The elevation estimation error in response to an elevation harmonic disturbance of amplitude 0.1 mdeg.

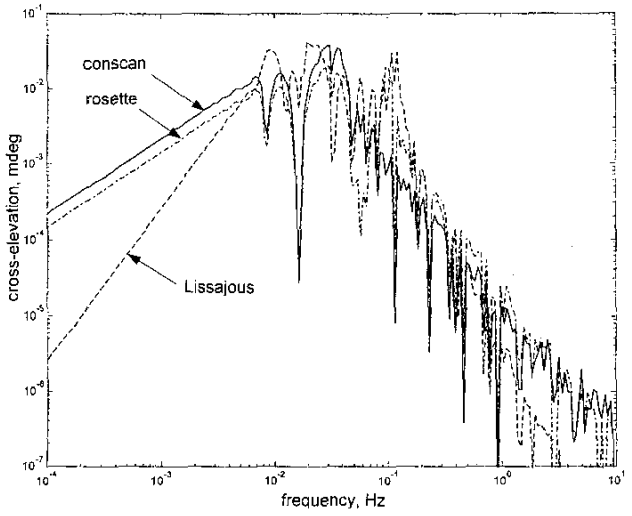

Figure 11b. The cross-elevation estimation error in response to an elevation harmonic disturbance of amplitude 0.1 mdeg.

spacecraft spinning. The latter disturbances are decomposed into harmonic components.

6.1 Position Disturbances

Position disturbances are caused by antenna motion. These disturbances may be purely random, and as such, they may be modeled as a white Gaussian noise of given standard deviation. Or, they may be more or less deterministic disturbances, which are modeled as harmonic components within a bandwidth up to 10 Hz (i.e., the antenna-dynamics bandwidth).

The random disturbances were simulated separately in the elevation and cross-elevation directions. The results are shown in Tables 1 and 2. They show that the scanning algorithms have quite effective disturbance-rejection properties. In conscan, for example, a disturbance in the XEL (cross-elevation) direction of 0.3 mdeg standard deviation will cause approximately 0.005 mdeg of error in the EL (elevation) estimation, and 0.01 mdeg of error in the XEL estimation.

The antenna position, x_a, was also disturbed by a harmonic motion in the EL direction, of frequency f and amplitude 0.1 mdeg. The disturbance's impact on estimation accuracy was analyzed for frequencies ranging from 0.0001 Hz (very slow motion) to 10 Hz (the antenna bandwidth). Note that the scanning frequency is $f_o = 1/60 = 0.0167$ Hz. Consider the plots of the estimation error in EL and XEL as shown in Figures 11a and 11b. They show that the disturbances are quickly suppressed for frequencies higher that the scanning frequency. The slope of the error magnitude drops as follows: for conscan, −60 dB/dec in EL and −40 dB/dec in XEL; for Lissajous scan, −20 dB/dec in EL and −60 dB/dec in XEL; and for rosette, −20 dB/dec in EL and −40 dB/dec in XEL. For low frequencies, the disturbance level is constant in EL for all scans, and drops down in XEL: −20 dB/dec for conscan and rosette scan, and −40 dB/dec for Lissajous scan.

When the harmonic disturbance is applied in cross-elevation, the picture is symmetric: whatever was said previously about estimation error in EL is now true for XEL, and vice versa.

6.2. Power Disturbances

Random power variation was also simulated. Variations had standard deviations ranging from 0.1% to 10% of maximum power. For all three scans, the EL and XEL estimation error was proportional to the variation of power with a gain of 0.080-0.089 mdeg per 10% of power variation, as shown in Table 3. This is very effective suppression of power noise, since the 10% standard deviation of power variation caused less than 0.1 mdeg estimation error.

Table 3. The estimation error (mdeg) due to power noise, , for spacecraft position at (0, 0). The standard deviation of the power noise was 10% of the peak power.

Direction	Conscan	Lissajous	Rosette
Elevation	0.089	0.083	0.080
Cross-elevation	0.089	0.080	0.088

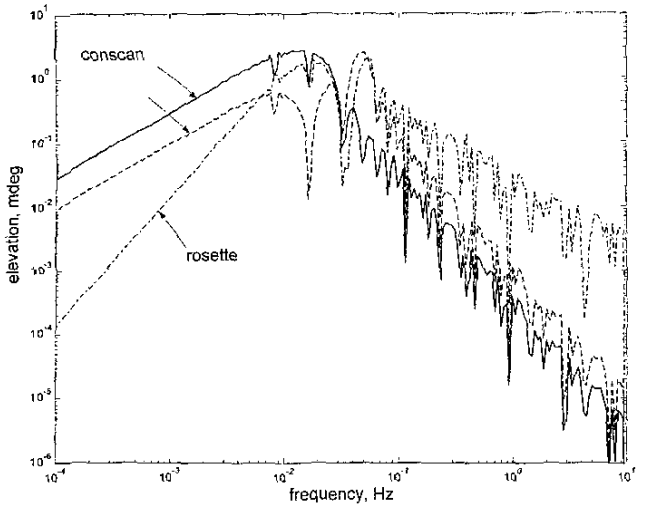

Figure 12a. The elevation estimation error in response to a harmonic power variation.

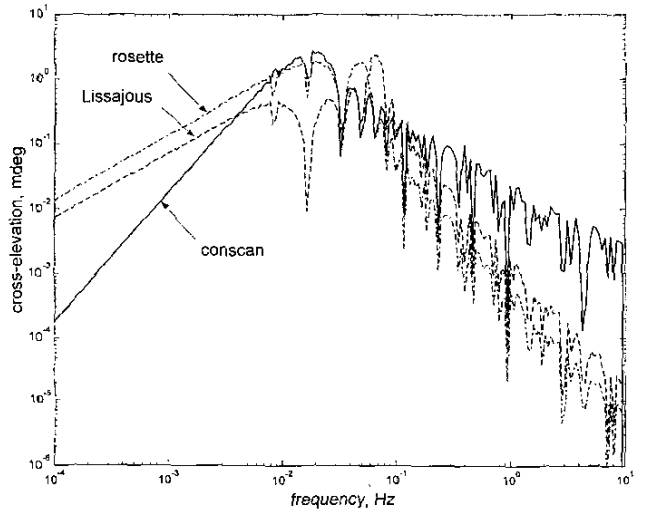

Figure 12b. The cross-elevation estimation error in response to a harmonic power variation.

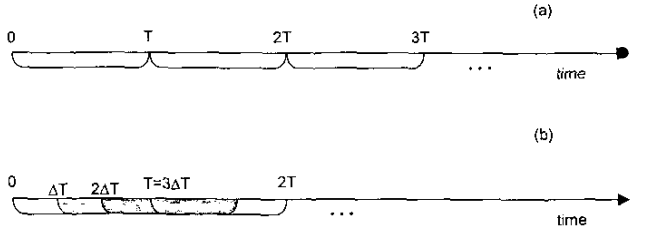

Figure 13. Non-sliding (a) and sliding-window (b) scans, for $\Delta T = \frac{1}{3}T$.

Next, the impact of pulsating power on the estimation of the EL and XEL position was analyzed. The results are shown in Figures 12a and 12b. The harmonic power variations were of frequencies ranging from 0.0001 Hz to 10 Hz, and of amplitude 0.1 (10% of maximum power). The plots show that the maximum estimation error of 3 mdeg amplitude was observed for frequencies near the scan frequency, and that for lower and higher frequencies, the amplitude of the estimation errors quickly dropped. Thus, all three scanning algorithms acted as effective filters for this kind of disturbance.

7. Sliding-Window Conscan

The spacecraft position-estimation technique described up to this point has used data collected during a single scanning period. Thus, the spacecraft position estimate is updated every period T, which typically ranges from 60 to 120 s. This is a rather slow update, which can cause a significant lag in the antenna tracking if the assumption of slowly varying target position is incorrect. This lag can be improved using a technique known as sliding-window scanning. In sliding-window scanning, the spacecraft position is estimated every time period, ΔT, where $\Delta T < T$. The update moments are shown in Figure 13 for $\Delta T = \frac{1}{3}T$. In this case, the data used in Equation (15) do not start at the beginning of every circle; rather, they begin at times T, $T+\Delta T$, $T+2\Delta T$, $T+3\Delta T$, etc. Note that the first estimation is at T rather than ΔT, because an entire circle is required to complete the estimation process. The data are collected for an entire circle, as shown in Table 4.

To see the usefulness of the sliding-window technique in the estimation process, assume that the target position changes rapidly by 0.15 mdeg at $t = 150$ s. This type of shift may be caused by a sudden disturbance in antenna position, such as a large gust of wind. This is an extreme situation, since in the closed-loop configuration, the control system would "soften" the impact of the gusts. The shift is illustrated in Figure 14, along with simulated

Table 4. The data collection time for the sliding-window scan.

Data Collection Time	Time Span of the Circle
T	$[0, T]$
$T+\Delta T$	$[\Delta T, T+\Delta T]$
$T+2\Delta T$	$[2\Delta T, T+2\Delta T]$
$T+i\Delta T$	$[i\Delta T, T+i\Delta T]$

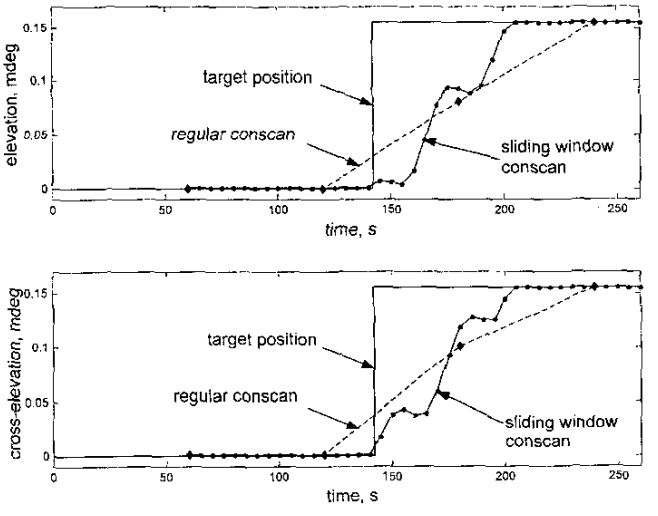

Figure 14. The estimated spacecraft position for a sliding-window conscan and for a non-sliding conscan.

responses of antennas using the traditional conscan method and the sliding-window method. The simulations show that for the conscan period $T = 60$ s, 120 s are required to reach the target, whereas the sliding-window conscan with $\Delta T = 5$ s reaches the target in half the time, i.e., in 60 s. This is especially important when antenna dynamics are involved, since faster sensors improve the pointing accuracy. Similar results were obtained for the Lissajous and rosette scans.

8. Conclusions

In this paper, three scanning techniques (conical, Lissajous, and rosette scans) were analyzed. It was shown that all of them have similar properties in the estimation accuracy of the spacecraft position for random and harmonic disturbances. Therefore, where the spacecraft angular position is concerned, the conscan should be chosen, due to its simplicity of implementation. Sliding-window scans were introduced and analyzed, and it was shown that they were significantly faster than non-sliding scans, while preserving other non-sliding-scan properties.

The algorithms presented here are based on the least-square conscan algorithm by Alvarez [4], and the Kalman algorithm by Eldred [5]. It should be noted that the two algorithms are similar, since both result from the assumption of the negligibility of the spacecraft movement with respect to the antenna position during the conscan period. It is a justified assumption, but the Kalman algorithm, in this case, becomes a least-square algorithm. It is also worth noticing that the Alvarez algorithm, unlike the Eldred algorithm, estimates the peak power of the signal in addition to the spacecraft position, but because there is interdependence between the power and spacecraft position, this algorithm can produce biased results.

9. Acknowledgement

The research described in this paper was carried out at the Jet Propulsion Laboratory, California Institute of Technology, under a contract with the National Aeronautics and Space Administration.

10. References

1. J. B. Damonte and D. J. Stoddard, "An Analysis of Conical Scan Antennas for Tracking," *IRE National Convention Record*, **4**, 1, 1956.

2. G. Biernson, *Optimal Radar Tracking Systems*, New York, Wiley, 1990.

3. J. E. Ohlson and M. S. Reid, "Conical-Scan Tracking with 64-m Diameter Antenna at Goldstone," *JPL Technical Report*, 32-1605, Jet Propulsion Laboratory, Pasadena, CA, October 23, 1976.

4. L. Alvarez, "Analysis of Open-Loop Conical Scan Pointing Error and Variance Estimators," The Telecommunications Mission Operations Progress Report 42-115, November 1993, Jet Propulsion Laboratory, Pasadena, CA; see http://tmo.jpl.nasa.gov/tmo/progress_report/42-115/115g.pdf.

5. D. B. Eldred, "An Improved Conscan Algorithm Based on Kalman Filter," The Telecommunications Mission Operations Progress Report 42-116, February 1994, Jet Propulsion Laboratory, Pasadena, CA; see http://tmo.jpl.nasa.gov/tmo/progress_report/42-116/116r.pdf.

6. H.-P. Lee and H.-Y Hwang, "Design of Two-Degree-of Freedom Robust Controllers for a Seeker Scan Loop System," *Int. Journal of Control*, **66**, 4, 1997.

7. H. Wan, Z. Liang, Q. Zhang, and X. Su, "A Double Band Infrared Image Processing System Using Rosette Scanning," in *Detectors, Focal Plane Arrays, and Applications, SPIE Proceedings*, **2894**, 1996.

Introducing the Feature Article Authors

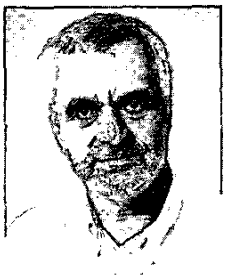

Wodek Gawronski received his MSc and PhD in mechanical engineering from the Technical University of Gdansk, Poland. He was a professor of dynamics and controls at the Technical University of Gdansk and at the University of Hanover, Germany. Later, he was a NRC Senior Fellow at the NASA Langley Research Center, Hampton, Virginia, working on spacecraft structural dynamics and control problems. Currently, he is Engineering Principal in the Communication Ground Systems Section, Jet Propulsion Laboratory, responsible for the control-system analysis and design of the NASA Deep Space Network antennas. He was also a consultant on control-system design to several radio telescope projects, including the NRAO 100-meter Green Bank Telescope, West Virginia, and the 50-meter Large Millimeter Wavelength Telescope in Pueblo, Mexico.

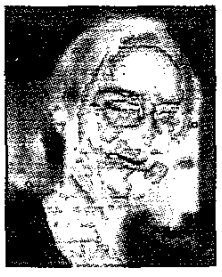

Emily Craparo is currently a graduate student in the Laboratory for Information and Decision Systems at the Massachusetts Institute of Technology, where she is funded through fellowships from the National Science Foundation and the Department of Defense. She performed the research described in this paper through NASA's Undergraduate Summer Research Program (USRP).